JOURNAL OF THERMOPHYSICS AND HEAT TRANSFER
Vol. 7, No. 2, April–June 1993

Refractive Index and Scattering Effects on Radiative Behavior of a Semitransparent Layer

C. M. Spuckler* and R. Siegel†
NASA Lewis Research Center, Cleveland, Ohio 44135

Heat transfer characteristics are analyzed for a plane layer of semitransparent material with refractive index ≥ 1. Energy transfer in the material is by conduction, emission, absorption, and isotropic scattering. The layer surfaces are diffuse intending to model a ceramic layer in high temperature applications. Each side of the layer is heated by radiation and convection. Internal reflections at the boundary surfaces are included. For a refractive index larger than unity, there is internal reflection of some of the energy within the layer. This, coupled with scattering, has a substantial effect on distributing energy across the layer and altering the temperature distribution from when the refractive index is unity. The effect of scattering is examined by comparisons with results from an earlier paper for an absorbing layer. Results are given for a gray medium with a scattering albedo up to 0.999, and for a two-band spectral variation of the albedo with one band having low absorption. Radiant energy leaving the surface as a result of emission and scattering was examined to determine if it could be used to accurately indicate the surface temperature.

Nomenclature

A = quantity defined in Eq. (11c)
a = absorption coefficient of layer, m^{-1}
C = quantity defined in Eqs. (11d) and (11e); $\bar{C} = C/\sigma T_{g1}^4$
C_2 = blackbody radiation constant, $m \cdot K$
c_0 = velocity of electromagnetic propagation in vacuum, m/s
D = thickness of plane layer, m
dq_ν = spectral flux in a differential interval of frequency, $W \cdot s/m^2$
E_1, E_2, E_3 = exponential integral functions, $E_n(x) = \int_0^1 \mu^{n-2} \exp(-x/\mu)\, d\mu$
$e_{\nu b}$ = blackbody hemispherical spectral radiation for $n = 1$, $W \cdot s/m^2$
$F_{0-\nu}$ = blackbody fraction in frequency range 0 to ν; F_k, for the kth band
H_R = dimensionless convection-radiation parameter, $h_1/\sigma T_{g1}^3$
h = convective heat transfer coefficient, $W/m^2 \cdot K$
I = radiative source function, W/m^2; $\bar{I} = \pi I/n^2 \sigma T_{g1}^4$
K = extinction coefficient, $a + \sigma_s$, m^{-1}
k = thermal conductivity of radiating medium, $W/m \cdot K$
N_D = conduction-radiation parameter based on length D, $k/\sigma T_{g1}^3 D$
n = index of refraction
q = heat flux, W/m^2; $\bar{q} = q/\sigma T_{g1}^4$
q_r = radiative heat flux, W/m^2
$q_{\nu r1}, q_{\nu r2}$ = spectral radiative heat fluxes incident from surroundings on each side, W/m^2
R = ratio of heat transfer coefficients, h_1/h_2
T = absolute temperature, K
T_g = gas temperature, K
T_{s1}, T_{s2} = temperatures of radiating surroundings, K
t = dimensionless temperature, T/T_{g1}
x = coordinate normal to boundary of plane layer, m; $X = x/D$
β = quantity defined in Eq. (21)
ε = emissivity of surface for an opaque layer
κ = optical coordinate $K \cdot x$; κ_D, optical thickness, $K \cdot D$
ν = frequency, s^{-1}
ρ^i = reflectivity of interface for internally incident radiation
ρ^o = reflectivity of interface for externally incident radiation
σ = Stefan-Boltzmann constant, $W/m^2 \cdot K^4$
σ_s = scattering coefficient, m^{-1}
τ^o = transmissivity of interface for externally incident radiation
Ω = scattering albedo, σ_s/K

Subscripts

a = apparent surface temperature from heat flux
g = gas on either side of layer
i, o = incoming and outgoing radiation
k = the kth frequency band
r = radiative quantity
ν = frequency
1, 2 = the hotter and cooler surroundings of the layer

Introduction

THIS analysis is a continuation of a previous study[1] to examine the effects of scattering in a plane layer of semitransparent ceramic material heated by radiation and convection. The previous analysis[1] showed that the temperature distribution in such a layer can be significantly influenced by its index of refraction. The amount of external radiant energy reflected from the outside surface and transmitted into the interior of a material depends on its refractive index. A more significant effect is that radiation emitted within the material volume depends on the square of its refractive index; the internal volume emission can therefore be many times that emitted by a blackbody radiating into a vacuum. Since radiation exiting from an interface cannot exceed that of a blackbody, there is extensive energy reflection at the internal interfaces, most of it by total internal reflection. The resulting effect on the layer temperature distribution was shown in Ref.

Received Feb. 17, 1992; revision received June 8, 1992; accepted for publication June 8, 1992.

*Research Scientist, Heat Transfer Branch.
†Research Scientist, Lewis Research Academy. Fellow AIAA.

1 for an absorbing layer; the effect of scattering is examined here. Scattering is another means for energy transfer in the layer, and further interacts with the effect of total reflection as the refractive index is increased.

The present analysis examines the effect of isotropic scattering on the heat transfer characteristics for various refractive indices and other independent parameters. The layer material, like many ceramics, has absorption and scattering coefficients that are functions of the radiation frequency. The analysis includes a spectrally dependent scattering albedo.

Results are shown first for a gray layer with various scattering albedos up to 0.999. Then a two-band spectral variation of the absorption coefficient is examined with an added gray component of scattering. The two-band model simulates the type of spectral variations reported for ceramics.[2] A larger number of bands can be included in the calculations if needed; the computer program is written for an arbitrary number of bands. The results for various refractive indices and scattering albedos include temperature distributions, surface temperatures, and apparent surface temperatures that an optical pyrometer would measure based on radiant energy received. The ceramic surfaces are assumed to have some roughness, so they act to diffuse transmitted or reflected radiation. Diffuse boundary conditions are used in the analysis. The layer reaches an equilibrium temperature distribution, depending on the surrounding heating or cooling environments that provide radiation and convection. The effects on the layer temperature distribution are investigated for various magnitudes of the heat transfer conditions.

An analysis of temperature distributions in absorbing-emitting layers, including index of refraction effects, was developed by Gardon[3] to predict cooling and heat treating of glass plates. The interfaces were optically smooth so reflections are specular and are computed from the Fresnel reflection laws. Another application[4] was for the heating of a window in a reentry vehicle. Recently, several papers[5-7] have further examined the effects of Fresnel boundary reflections and nonunity refractive index. In other instances, diffuse assumptions at the interfaces have been used in analyses of steady and transient heat transfer to single or multiple plane layers.[8-10] Reference 11 includes both spectral and directional effects at solid walls bounding a semitransparent layer. Directional variations of the emission-reflection characteristics of the bounding solid walls were found to have small effects. The present authors have not found a detailed analysis for a scattering layer subjected to the heating conditions studied here. This includes the effects of diffuse interfaces without enclosing solid boundaries, the total reflection of a portion of the internally radiated energy, isotropic scattering, and a nonunity refractive index. The analysis is given for a general spectral variation in both the absorption and scattering coefficients.

Analysis

The geometry and coordinate system are in Fig. 1. The layer has thickness D, constant n, and spectral absorption and scattering coefficients a_ν and $\sigma_{s\nu}$. A specified spectral distribution of diffuse radiative heat fluxes $dq_{\nu r1}(\nu)$ and $dq_{\nu r2}(\nu)$ is incident on each boundary, and there is convective heat transfer provided by external gas flows at temperatures T_{g1} and T_{g2} with h_1 and h_2. Side 1 is selected as the higher temperature side.

Temperature Distribution Relations from Energy Equation

Within the semitransparent material, energy is transferred by conduction and radiation. The radiative energy flux is written as the integral over all frequencies of the spectral flux so that the energy equation is[12]

$$k\frac{d^2T}{dx^2} - \frac{d}{dx}\int_{\nu=0}^{\infty} dq_{\nu r}(x, \nu) = 0 \tag{1}$$

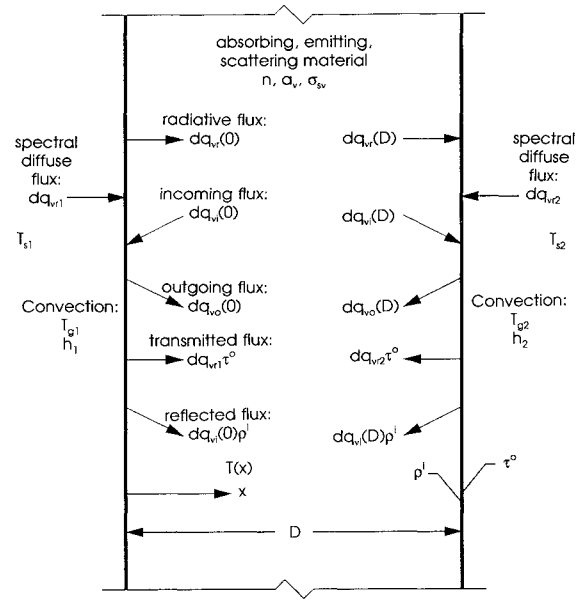

Fig. 1 Geometry, coordinate system, and nomenclature for radiative fluxes for absorbing and scattering layer.

Equation (1) is integrated with respect to x and equated to its values at $x = 0$ and D to give

$$k\left.\frac{dT}{dx}\right|_x - \int_0^\infty dq_{\nu r}(x, \nu) = \text{const}$$

$$= k\left.\frac{dT}{dx}\right|_0 - \int_0^\infty dq_{\nu r}(0, \nu) = k\left.\frac{dT}{dx}\right|_D - \int_0^\infty dq_{\nu r}(D, \nu) \tag{2}$$

Each boundary is exposed to diffuse radiation incident from the surroundings and to convection. After partial reflection at a boundary, radiation passes into the medium and interacts internally. There is no absorption at the plane of the interface since it does not have any volume. Hence, the conduction derivative terms at the boundaries equal only the convection, so that Eq. (2) becomes

$$-k\left.\frac{dT}{dx}\right|_x + \int_0^\infty dq_{\nu r}(x, \nu) = h_1[T_{g1} - T(0)]$$

$$+ \int_0^\infty dq_{\nu r}(0, \nu) = h_2[T(D) - T_{g2}] + \int_0^\infty dq_{\nu r}(D, \nu) \tag{3}$$

As shown in Ref. 1 the energy equation in the form of Eq. (3) is integrated again, with respect to x, and the following relations are obtained for the layer temperature distribution and surface temperatures

$$T(x) = T(0) - \frac{h_1}{k}[T_{g1} - T(0)]x$$

$$- \frac{x}{k}\int_0^\infty dq_{\nu r}(0, \nu) + \frac{1}{k}\int_0^x \left[\int_0^\infty dq_{\nu r}(x, \nu)\right] dx \tag{4}$$

$$T(0) = T_{g1} + \left[\frac{h_1}{h_2} + 1 + \frac{h_1 D}{k}\right]^{-1}\left\{T_{g2} - T_{g1}\right.$$

$$+ \left[\frac{1}{h_2} + \frac{D}{k}\right]\int_0^\infty dq_{\nu r}(0, \nu) - \frac{1}{h_2}\int_0^\infty dq_{\nu r}(D, \nu)$$

$$\left. - \frac{1}{k}\int_0^D \left[\int_0^\infty dq_{\nu r}(x, \nu)\right] dx\right\} \tag{5}$$

$$T(D) = T(0) + \frac{h_1}{h_2}[T_{g1} - T(0)] + \frac{1}{h_2}\int_0^\infty dq_{\nu r}(0, \nu) - \frac{1}{h_2}\int_0^\infty dq_{\nu r}(D, \nu) + [T_{g1} - T(0)] + (T_{g2} - T_{g1}) \quad (6)$$

Relations for Radiative Flux

Equations (4) and (5) for the temperature distribution contain the spectral radiative flux, $dq_{\nu r}(x, \nu)$. For a medium with scattering, this depends on the unknown radiative source function $I_\nu(x, \nu)$, and is given in $d\nu$ for a plane layer by[12]

$$\frac{dq_{\nu r}(x)}{d\nu} = 2\frac{dq_{\nu o}(0)}{d\nu}E_3(K_\nu x) - 2\frac{dq_{\nu o}(D)}{d\nu}E_3[K_\nu(D - x)] + 2\pi K_\nu\left[\int_0^x I_\nu(x^*)E_2[K_\nu(x - x^*)]\,dx^* - \int_x^D I_\nu(x^*)E_2[K_\nu(x^* - x)]\,dx^*\right] \quad (7)$$

Equation (7) contains the diffuse spectral fluxes $dq_{\nu o}(0)$ and $dq_{\nu o}(D)$ in $d\nu$ that leave the internal surface of each boundary (Fig. 1). These fluxes must be expressed in terms of the fluxes incident from outside the layer to provide coupling with the externally imposed radiative conditions.

By using the procedure in Ref. 1, the boundary relations (see Fig. 1)

$$dq_{\nu o}(0) = dq_{\nu r1}\tau_\nu^o + dq_{\nu i}(0)\rho_\nu^i \quad (8a)$$

$$dq_{\nu o}(D) = dq_{\nu r2}\tau_\nu^o + dq_{\nu i}(D)\rho_\nu^i \quad (8b)$$

$$dq_{\nu r}(0) = dq_{\nu o}(0) - dq_{\nu i}(0) \quad (9a)$$

$$dq_{\nu r}(D) = -dq_{\nu o}(D) - dq_{\nu i}(D) \quad (9b)$$

were used to obtain the internal incoming fluxes

$$dq_{\nu i}(0) = 2\,dq_{\nu o}(D)E_3(K_\nu D) + 2\pi\int_0^D K_\nu I_\nu(x)\,d\nu E_2(K_\nu x)\,dx \quad (10a)$$

$$dq_{\nu i}(D) = 2\,dq_{\nu o}(0)E_3(K_\nu D) + 2\pi\int_0^D K_\nu I_\nu(x)\,d\nu E_2[K_\nu(D - x)]\,dx \quad (10b)$$

The $dq_{\nu i}(0)$ and $dq_{\nu i}(D)$ are eliminated between Eqs. (8) and (10), and the resulting simultaneous equations solved for $dq_{\nu o}(0)/d\nu$ and $dq_{\nu o}(D)/d\nu$ (the ratios relative to $d\nu$ are used to avoid dealing numerically with infinitesimal quantities such as dq_ν)

$$\frac{dq_{\nu o}(0)}{d\nu} = \frac{C_{\nu 1}/d\nu + A_\nu C_{\nu 2}/d\nu}{1 - A_\nu^2} \quad (11a)$$

$$\frac{dq_{\nu o}(D)}{d\nu} = \frac{C_{\nu 2}/d\nu + A_\nu C_{\nu 1}/d\nu}{1 - A_\nu^2} \quad (11b)$$

where

$$A_\nu = 2\rho_\nu^i E_3(K_\nu D) \quad (11c)$$

$$\frac{C_{\nu 1}}{d\nu} \equiv \tau_\nu^o\frac{dq_{\nu r1}}{d\nu} + 2\rho_\nu^i\pi K_\nu\int_0^D I_\nu(x)E_2(K_\nu x)\,dx \quad (11d)$$

$$\frac{C_{\nu 2}}{d\nu} \equiv \tau_\nu^o\frac{dq_{\nu r2}}{d\nu} + 2\rho_\nu^i\pi K_\nu\int_0^D I_\nu(x)E_2[K_\nu(D - x)]\,dx \quad (11e)$$

Equation for the Source Function

The radiative flux depends on the source function $I_\nu(x)$. This is obtained from the integral equation for a plane layer[12]

$$I_\nu(x) = (1 - \Omega_\nu)n^2\frac{e_{\nu b}(x)}{\pi} + \frac{\Omega_\nu}{2}\left\{\frac{dq_{\nu o}(0)}{\pi\,d\nu}E_2(K_\nu x) + \frac{dq_{\nu o}(D)}{\pi\,d\nu}E_2[K_\nu(D - x)] + K_\nu\int_0^D I_\nu(x^*)E_1(K_\nu|x - x^*|)\,dx^*\right\} \quad (12)$$

Solution Procedure

An iterative solution is obtained by assuming temperature and spectral source function distributions as a first step. To resolve the spectral dependence, a sufficient number of frequency values are needed to provide the desired accuracy when a numerical integration is carried out over frequency to obtain the total energy. For each ν the A_ν, $C_{\nu 1}/d\nu$, and $C_{\nu 2}/d\nu$ are evaluated from Eqs. (11c), (11d), and (11e) and are used to calculate $dq_{\nu o}/d\nu$ from Eqs. (11a) and (11b). New $I_\nu(x)$ are then obtained by iterating Eq. (12) for each ν where $e_{\nu b}(x)$ is evaluated using the assumed $T(x)$. The $dq_{\nu r}(x)/d\nu$ is then obtained from Eq. (7). $T(0)$ is evaluated from Eq. (5), and a new temperature distribution $T(x)$ is obtained from Eq. (4). This temperature distribution along with the spectral and spatial distributions of $I_\nu(x)$ are used to start a new iteration. The process is continued until a converged solution is obtained. The procedure is now given for a banded solution, which is the usual solution method.

Relations for Frequency Banded Model in Dimensionless Form

In a banded formulation, the extinction coefficient and scattering albedo have constant values in each designated spectral range. The K_k and Ω_k apply in the kth frequency band from ν_k to ν_{k+1}. If τ_ν^o and ρ_ν^i vary with frequency, they are also approximated as constant within each band. The preceding relations are integrated over the kth band, and using the groups defined in the nomenclature, the band equations needed for the iterative solution have the dimensionless forms.

Boundary relations

$$\Delta\tilde{q}_{ko}(0) = \frac{\tilde{C}_{k1} + A_k\tilde{C}_{k2}}{1 - A_k^2} \quad (13a)$$

$$\Delta\tilde{q}_{ko}(1) = \frac{\tilde{C}_{k2} + A_\nu\tilde{C}_{k1}}{1 - A_k^2} \quad (13b)$$

$$A_k = 2\rho_k^i E_3(\kappa_{Dk}) \quad (13c)$$

$$\tilde{C}_{k1} = \tau_k^o\Delta\tilde{q}_{kr1} + 2n^2\rho_k^i\kappa_{Dk}\int_0^1 \Delta\tilde{I}_k(X)E_2(\kappa_{Dk}X)\,dX \quad (13d)$$

$$\tilde{C}_{k2} = \tau_k^o\Delta\tilde{q}_{kr2} + 2n^2\rho_k^i\kappa_{Dk}\int_0^1 \Delta\tilde{I}_k(X)E_2[\kappa_{Dk}(1 - X)]\,dX \quad (13e)$$

Source function equation

$$\Delta\tilde{I}_k(X) = (1 - \Omega_k)t^4(X)F_k(T) + \frac{\Omega_k}{2}\left\{\frac{\Delta\tilde{q}_{ko}(0)}{n^2}E_2(\kappa_{Dk}X) + \frac{\Delta\tilde{q}_{ko}(1)}{n^2}E_2[\kappa_{Dk}(1 - X)] + \kappa_{Dk}\int_0^1 \Delta\tilde{I}_k(X^*)E_1(\kappa_{Dk}|X - X^*|)\,dX^*\right\} \quad (14)$$

The $F_k(T)$ is the energy fraction in the kth frequency band for a blackbody at temperature $T(x)$.

Flux relations

$$\Delta\tilde{q}_{kr}(X) = 2\Delta\tilde{q}_{ko}(0)E_3(\kappa_{kD}X) - 2\Delta\tilde{q}_{ko}(1)E_3[\kappa_{kD}(1 - X)] + 2\kappa_{kD}n^2\left\{\int_0^X \Delta\tilde{I}_k E_2[\kappa_{kD}(X - X^*)]\,dX^* - \int_X^1 \Delta\tilde{I}_k E_2[\kappa_{kD}(X^* - X)]\,dX^*\right\} \quad (15)$$

Each integration over frequency in Eq. (4) is obtained as a sum over the spectral bands

$$\tilde{q}_r(X) = \sum_k \Delta\tilde{q}_{kr}(X) \quad (16)$$

Temperature relations

$$t(0) = 1 + \left(R + 1 + \frac{H_R}{N_D}\right)^{-1}\left\{t_{g2} - 1 + \frac{1}{H_R}\left[\left(R + \frac{H_R}{N_D}\right)\tilde{q}_r(0) - R\tilde{q}_r(1) - \frac{H_R}{N_D}\int_0^1 \tilde{q}_r(X)\,dX\right]\right\} \quad (17)$$

$$t(X) = t(0) - \frac{1}{N_D}\left\{H_R[1 - t(0)]X - \tilde{q}(0)X + \int_0^X \tilde{q}_r(X)\,dX\right\} \quad (18)$$

Relations for Diffuse Interface Transmittance and Reflectance

For diffuse interfaces, the roughness influences τ^o for radiation incident from the outside, and ρ^i for radiation incident from within the layer. When the refractive index of the medium is greater than unity, ρ^i must account for some of the internal radiation being totally reflected at the interface.

In the absence of other information, the interface characteristics for a ceramic surface were determined by integrated averages of the Fresnel reflection relations. For diffuse externally incident radiation this gives[12]

$$\tau^o(n) = 1 - \rho^o(n) = \frac{1}{2} - \frac{(3n + 1)(n - 1)}{6(n + 1)^2} - \frac{n^2(n^2 - 1)^2}{(n^2 + 1)^3}\,\ell n\left(\frac{n - 1}{n + 1}\right) + \frac{2n^3(n^2 + 2n - 1)}{(n^2 + 1)(n^4 - 1)} - \frac{8n^4(n^4 + 1)}{(n^2 + 1)(n^4 - 1)^2}\,\ell n(n) \quad (19)$$

This assumes the interface properties can be calculated by considering the medium to be a nonattenuating dielectric, that is, neglecting the effect of the extinction coefficient in the complex index of refraction. This is reasonable unless the extinction coefficient is large.[13] For spectral regions where there is a high extinction coefficient, relations must be used to obtain τ^o and ρ^i that include the imaginary part of the complex index of refraction (Ref. 12, Chap. 4). After allowing for energy at angles larger than the critical angle for total reflection, the $\rho^i(n)$ is found from[14]

$$\rho^i(n) = 1 - [\tau^o(n)/n^2] \quad (20)$$

Values of $\tau^o(n)$ and $\rho^i(n)$ are in Table 1 of Ref. 1 for various n. The internal reflection becomes large as n increases.

Numerical Solution Method

The numerical solution of Eq. (14) for $\Delta\tilde{I}_k(X)$ in each wavelength band requires integrating $\Delta\tilde{I}_k(X)$ multiplied by E_1. Since $E_1(0) \to \infty$ the integrals were evaluated analytically for a small region where X^* is near X by using $\Delta\tilde{I}_k(X^*) \approx \Delta\tilde{I}_k(X)$ which is then taken out of the integral. The integral of E_1 with respect to X^* is then done analytically. The rest of the integral was evaluated with the Gaussian integration subroutine QDAGS from the IMSL library. The layer was divided into evenly spaced grid points; by trying various grid sizes, 41 points were usually found sufficient so that more points did not change the temperature distributions more than a fraction of 1%. For an optical thickness of 100 some calculations were made with 81 points. The $\Delta\tilde{I}_k(X)$ and $t^4(X)$ distributions were fitted during each iteration by the cubic spline subroutine CSINT from the IMSL library. The Gaussian subroutine called for unevenly spaced grid points, and during the calculations they were interpolated as required from the spline fit.

The blackbody fraction $F_k(T) = F_{0-\nu_{k+1}}(T) - F_{0-\nu_k}(T)$ in Eq. (14) was evaluated during the solution by using the rapidly converging series[15]

$$F_{0-\nu}(T) = 1 - \frac{15}{\pi^4}\sum_m \frac{e^{-m\beta}}{m}\left(\beta^3 + \frac{3\beta^2}{m} + \frac{6\beta}{m^2} + \frac{6}{m^3}\right)$$

where

$$\beta = C_2\nu/c_oT \quad (21)$$

Special Cases for Nonabsorbing and Opaque Layers

In the limit of zero absorption there is no radiative interaction with the temperature distribution, and the ordinary relations for heat flow through a plane layer with boundary convection and internal conduction are

$$t(0) = 1 - \frac{1 - t_{g2}}{1 + (H_R/N_D) + R} \quad (22a)$$

$$t(X) = t(0) - (H_R/N_D)[1 - t(0)]X \quad (22b)$$

For an opaque layer ($\kappa_D \to \infty$ with aD finite) there is absorption and emission only at the boundaries and $t(X)$ is linear. For opaque surfaces ε_1 and ε_2 depend on n and are equal to $1 - \rho^o = \tau^o$ from Eq. (19). The $t(0)$ and $t(1)$ are obtained from three equations: Eqs. (23a) and (23c) are from a heat balance at each gray interface, and Eq. (23b) is for internal heat conduction

$$H_R[1 - t(0)] + \varepsilon_1[\tilde{q}_{r1} - t^4(0)] - \tilde{q} = 0 \quad (23a)$$

$$N_D[t(0) - t(1)] - \tilde{q} = 0 \quad (23b)$$

$$(H_R/R)[t(1) - t_{g2}] + \varepsilon_2[t^4(1) - \tilde{q}_{r2}] - \tilde{q} = 0 \quad (23c)$$

Results and Discussion

The effect of the index of refraction on the temperature distribution was examined by Spuckler and Siegel[1] for a layer with absorption and emission; the present results show the additional effect of scattering. Results are given first for a gray layer; the effect of spectral property variations is then examined with two-band calculations. To reduce the parametric study the results given here are for $R = h_1/h_2 = 1$ and $t_{g2} = T_{g2}/T_{g1} = 0.25$. The surrounding temperatures are set equal to the gas temperatures; $t_{s1} = t_{g1} = 1$ and $t_{s2} = t_{g2} = 0.25$. The surroundings are assumed to act like blackbody sources so $q_{r1} = \sigma T_{s1}^4 = \sigma T_{g1}^4$ and $q_{r2} = \sigma T_{s2}^4 = \sigma T_{g2}^4$.

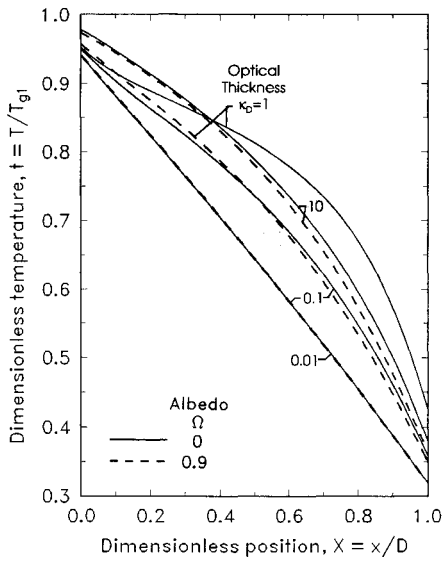

a) $n = 1$

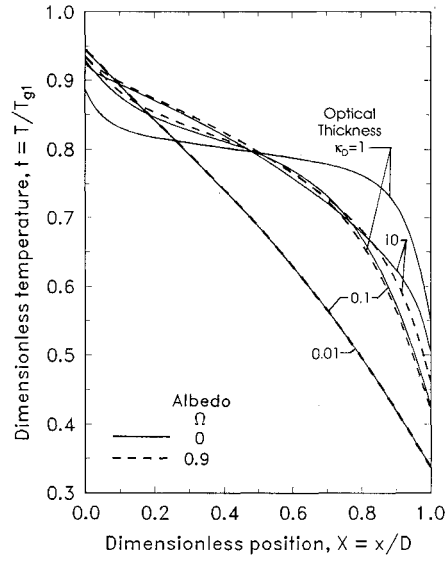

b) $n = 2$

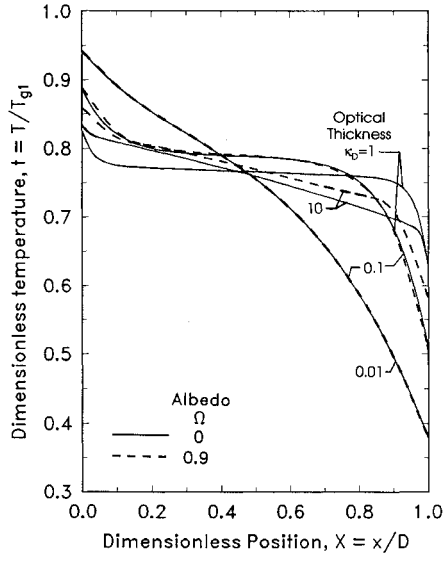

c) $n = 4$

Fig. 2 Effect of scattering albedo, optical thickness, and index of refraction on temperature distributions; $t_{s1} = t_{g1} = 1$, $t_{s2} = t_{g2} = 0.25$, $N_D = 0.1$, $H_R = 1$, $R = 1$.

Effect of Optical Thickness for Various Refractive Indices

In Fig. 2 temperature profiles for a gray layer with a scattering albedo of 0.9 are compared for various optical thicknesses with those for absorption alone. The three parts of the figure are for refractive indices, $n = 1$, 2, and 4. Convection is comparable to the external radiation at the hot side, so the convection-radiation parameter $H_R = 1$. The conduction parameter is rather small, $N_D = 0.1$; this provides a significant influence of internal radiation rather than the temperature distribution being dominated by conduction.

Compare the dashed curves for $\Omega = 0.9$ with the solid curves for $\Omega = 0$ (absorption only). The ratio of absorption to extinction is $a/(a + \sigma_s) = 1 - \Omega$, so for $\Omega = 0.9$, $aD = 0.1(a + \sigma_s)D$. For all three refractive indices, the temperature profiles for scattering with $\Omega = 0.9$ and optical thicknesses of $\kappa_D = (a + \sigma_s)D = 0.1$ and 1 are almost the same as those without scattering ($\Omega = 0$) and with optical thicknesses based only on the absorption thickness, $\kappa_D = aD = 0.01$ and 0.1. This shows that for an optical thickness, $(a + \sigma_s)D \leq 1$, it is absorption that dominates the temperature distribution; the presence of isotropic scattering has little effect and the profiles depend mainly on the absorption thickness aD. Looking in detail at the profiles, for $\Omega = 0.9$ and $\kappa_D = 1$, scattering produces only slight differences from the $t(X)$ obtained for $\kappa_D = 0.1$ with $\Omega = 0$. For small X, the profiles with scattering are slightly higher than those without scattering and with the same amount of absorption; for large X, however, the relative positions are reversed. For small X there is evidently absorption of backscattered energy. At large X scattering reduces the energy propagating forward from the hot side.

In contrast with the results for $\kappa_D \leq 1$, the temperature profiles for $\Omega = 0.9$ and $\kappa_D = 10$ ($aD = 1$) are close to those for $\Omega = 0$ and $aD = 10$. For this larger optical thickness, scattering enhances the absorption process and tends to act the same as absorption; for $0 \leq \Omega \leq 0.9$ with $\kappa_D = 10$ absorption is large enough to absorb the scattered energy instead of letting it pass through the layer. For $\kappa_D = 10$, the albedo must be larger than 0.9 for the profile to be significantly changed from that with $\Omega = 0$. This is shown in Fig. 3.

Effect of Large Scattering Albedo

The effect of large albedos $\Omega > 0.9$ is shown in Figs. 3 and 4 in two different ways. In Fig. 3 the optical thickness is kept at a fixed value $(a + \sigma_s)D = 10$. Therefore, as Ω is increased, there is proportionately less absorption and more scattering. As Ω goes to unity, and hence $a \to 0$, the temperature profile approaches the transparent limit in Eq. (22) as there is no

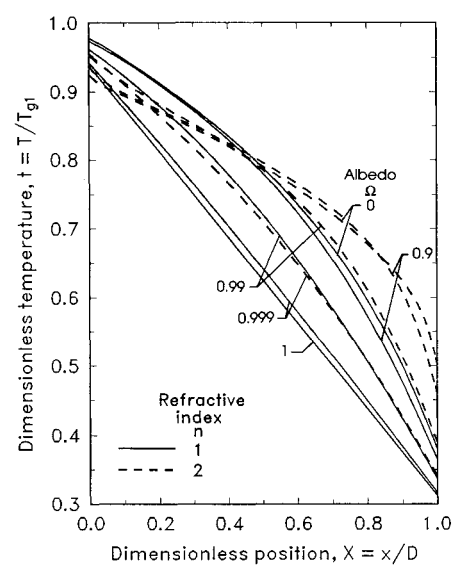

Fig. 3 Effect of large scattering albedos and index of refraction on temperature distributions for an optical thickness of 10; $t_{s1} = t_{g1} = 1$, $t_{s2} = t_{g2} = 0.25$, $N_D = 0.1$, $H_R = 1$, $R = 1$.

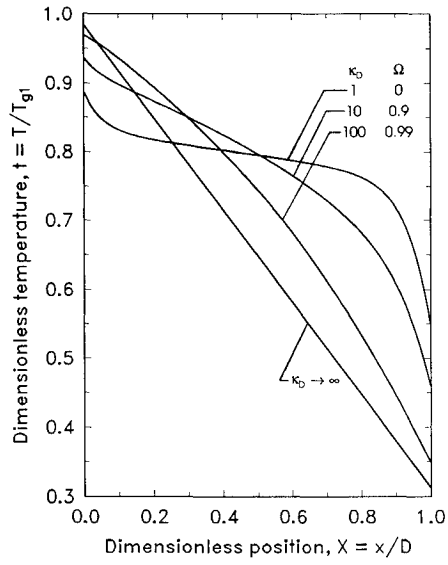

a) $aD = 1$

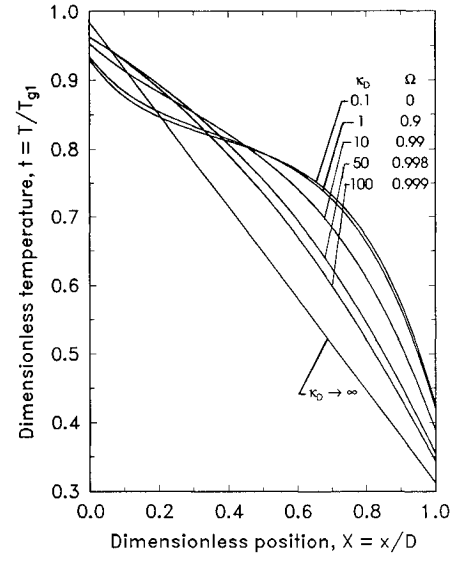

b) $aD = 0.1$

Fig. 4 Effect of increasing scattering while keeping absorption constant; $t_{s1} = t_{g1} = 1$, $t_{s2} = t_{g2} = 0.25$, $N_D = 0.1$, $H_R = 1$, $R = 1$, $n = 2$.

radiant absorption to interact with the local energy distribution. For each part of Fig. 4, however, aD, is held constant. The Ω is increased by adding scattering. For very large scattering $\sigma_s >> a$, $a + \sigma_s \approx \sigma_s$, and $\Omega \rightarrow 1$, but there is still finite absorption. The purpose of Fig. 4 is to show the effect of opacifying a layer with additional scattering σ_s, but without changing a.

In Fig. 3 for $\kappa_D = 10$ held fixed, the effect of albedos larger than 0.9 is shown for refractive indices of 1 (solid lines) and 2 (dashed lines). The conduction and convection parameters, $N_D = 0.1$ and $H_R = 1$, are the same as in Fig. 2. Consider the results for $n = 1$ (solid lines). As discussed in Fig. 2, for $\kappa_D = 10$ increasing Ω from 0 to 0.9 causes only a small change in the temperature profiles. For $\Omega = 0.99$, however, absorption is decreased sufficiently so that the temperature profile moves toward the transparent limit, Eq. (22), that is reached when $\Omega = 1$ and $a = 0$. The temperature profile is close to that in Fig. 2a for no scattering and for $aD = (1 - \Omega)\kappa_D = 0.1$. This indicates that for large scattering with small absorption the temperature profiles depend on aD rather than on $(a + \sigma_s)D$. When Ω is increased to 0.999 so that $aD = 0.001$, the temperature profile in Fig. 3 is practically at the transparent limit.

The results change somewhat for $n = 2$ in Fig. 3 (dashed lines). The temperature profiles are less linear than for $n = 1$. The profiles cross, and the crossover location moves to smaller X as Ω is increased. The internal reflection of scattered energy at the interfaces aids absorption within the layer, so as Ω is increased and aD becomes small, the profiles do not approach the transparent limit as rapidly as they did for $n = 1$.

In Fig. 4a, aD is kept fixed at 1 while Ω is increased. Hence, as Ω increases, the optical thickness $(a + \sigma_s)D$ increases. The effect of additional scattering with a fixed aD causes the temperature profile to move gradually toward the opaque limit given by Eqs. (23). These results are for $n = 2$.

Figure 4b shows the effect of a smaller absorption thickness, $aD = 0.1$. The aD is kept fixed and scattering is added. The behavior is similar to Fig. 4a except that the opaque limit is approached more slowly as κ_D increases. This is because there is very little absorption to influence the temperature distribution. Scattering increases multiple reflections within the layer and makes absorption more effective, so the opaque limit is gradually approached as scattering is added, while aD is kept constant.

Effect of Internal Heat Conduction

The effect of N_D, which is proportional to internal heat conduction, is shown in Fig. 5. The results are for $\kappa_D = 1$ where, for absorption alone, there was found to be a maximum internal radiative effect.[1] The heavy lines (both solid and dashed) are for $N_D = 0.1$: the thinner lines (solid and dashed) are for $N_D = 10$. The dashed lines are for $\Omega = 0.9$ and can be compared with the solid lines for $\Omega = 0$. Results are given for three refractive indices, $n = 1$, 2, and 4.

Figure 5 contrasts the behavior for $N_D = 0.1$ and 10 when Ω changes from 0 to 0.9 for a constant optical thickness $\kappa_D = 1$. Consider first the results for $\Omega = 0$. For $N_D = 10$, conduction is high enough that the temperature distributions are practically uniform; there is little effect of n on the profile shape. For $N_D = 0.1$, however, the profiles become more uniform in the central portion of the layer as n is increased. For a large n, energy is distributed across the layer by means of internal reflections. When Ω is increased from 0 to 0.9 (aD decreases from 1 to 0.1) the temperatures for $N_D = 10$ are decreased as a result of reduced absorption. The temperature profiles for $N_D = 0.1$ become less radiation-dominated because of decreased absorption, and have the more linear character of a conduction profile.

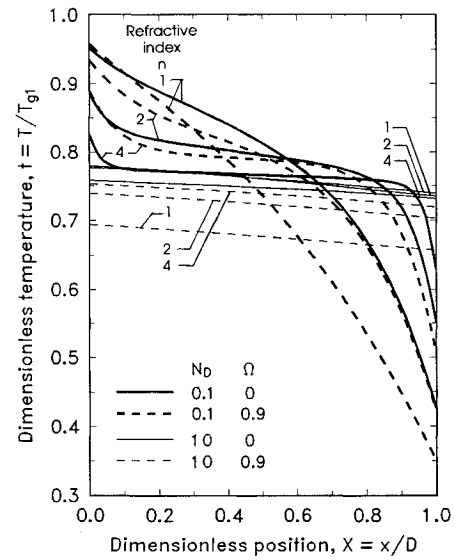

Fig. 5 Effect of heat conduction, scattering albedo, and index of refraction on temperature distributions; $t_{s1} = t_{g1} = 1$, $t_{s2} = t_{g2} = 0.25$, $H_R = 1$, $R = 1$, $\kappa_D = 1$.

Effect of Convection at Interfaces

The results in Figs. 2–5 are for an intermediate value of the convection parameter, $H_R = 1$. Figure 6 gives results for larger and smaller convection for an intermediate optical thickness, $\kappa_D = 1$. A large H_R (heavy solid and dashed lines on Fig. 6) causes the surface temperatures to move toward the gas temperatures (1 and 0.25). As n is increased, the temperature profiles become more uniform in the central region of the layer, and large gradients occur near the surfaces. The temperature uniformity in the central portion is produced by internal reflections that distribute energy across the layer. For small convection (thin solid and dashed lines in Fig. 6) the profiles become more uniform as n is increased. Radiation is dominating, and convection is insufficient to bring the surface temperatures near the gas temperatures. When Ω is increased from 0 to 0.9 (aD decreases from 1 to 0.1) the profiles show the effect of decreased absorption, and the layer tends to behave like one with absorption only with $aD = 0.1$ as discussed for Fig. 2 with $\kappa_D = 1$. For $n = 1$ and $H_R = 0.1$ the temperatures are reduced, but the profiles are similar. For $n = 2$ and 4 the temperatures are reduced at large X. For $\Omega = 0.9$ the temperature profiles tend to be less uniform in the central region than for $\Omega = 0$.

Surface Temperature and Apparent Surface Temperature Calculated from Radiative Energy Leaving Interface

When using radiation measurements to determine temperatures of semitransparent layers, radiant energy leaving the layer is detected and converted to an indicated surface temperature. The detected radiation consists of emitted, transmitted, scattered, and reflected energy. A correction is usually made to account for the energy reflected from the observed surface. The leaving flux used to determine the apparent surface temperature is emission and scattering by the layer combined with the flux transmitted through the layer from that supplied to the other side. The diffuse surface emissivity is equal to τ^o as obtained from Eq. (19) so T_a = (leaving flux/$\tau^o\sigma)^{1/4}$. In Fig. 7 the apparent surface temperature $t_a = T_a/T_{g1}$ is compared to the actual surface temperature from the distributions in the previous figures. Figure 7 gives results for $\Omega = 0$ (solid lines) and 0.9 (dashed lines) with a conduction parameter of $N_D = 0.1$; the two parts of the figure are for $n = 1$ and 2.

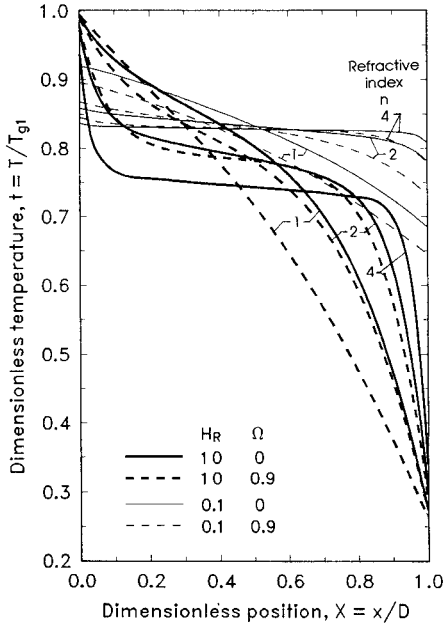

Fig. 6 Effect of convection, scattering albedo, and refractive index on temperature distributions; $t_{s1} = t_{g1} = 1$, $t_{s2} = t_{g2} = 0.25$, $N_D = 0.1$, $R = 1$, $\kappa_D = 1$.

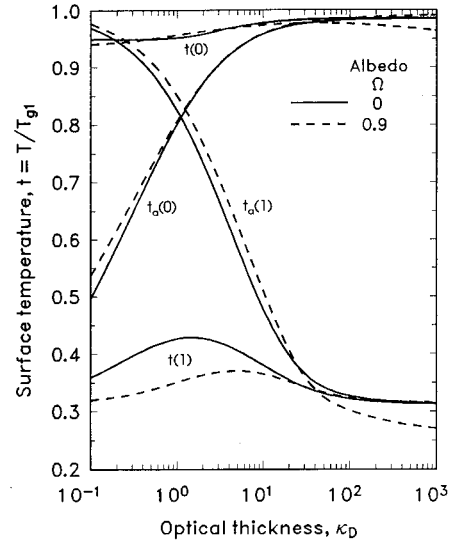

a) $n = 1$

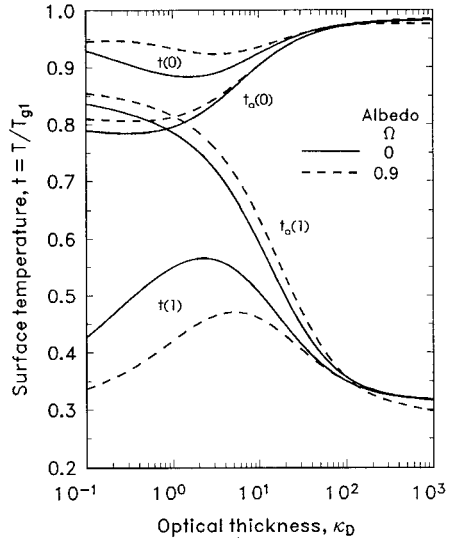

b) $n = 2$

Fig. 7 Effect of optical thickness, scattering, and refractive index on apparent surface temperatures computed from radiative flux; $t_{s1} = t_{g1} = 1$, $t_{s2} = t_{g2} = 0.25$, $H_R = 1$, $N_D = 0.1$, $R = 1$.

For the hot surface, when $n = 1$ the actual temperatures for $\Omega = 0.9$ are close to those for $\Omega = 0$ although when $\kappa_D > 10$ the difference increases. When $n = 2$ the $\Omega = 0.9$ results are higher than those for $\Omega = 0$ when $\kappa_D < 20$. For the cold side, the actual surface temperatures for $\Omega = 0.9$ are lower than those for $\Omega = 0$, but when κ_D is greater than about 20 there is little difference.

Comparing apparent and actual surface temperatures indicates that for $\Omega = 0$ fairly accurate surface temperature measurements can be made if $\kappa_D > 10$ for the hot surface and >30 for the cold surface. For $\Omega = 0.9$ the t_a and t curves cross and move apart at large κ_D. Scattered energy causes the energy leaving the surface to differ from that characteristic of the surface temperature. To obtain an accurate surface temperature a scattering correction may be required that depends on n. For $N_D = 1$ and $\Omega = 0$ it was found in Ref. 1 that the required κ_D are lower; the hot and cold surfaces now require $\kappa_D > 10$ if $\Omega = 0$.

Nongray Effects on Temperature Distributions

The previous results have been for a gray layer, and they provide insight into the behavior of a nongray layer. Some results are given here for a two-band model where the layer

optical thickness changes in a step fashion from a small to a larger value as wavelength is increased (frequency is decreased). The absorption coefficient has different values on either side of the cutoff wavelength with the lower value below the cutoff as is typical of window materials. Added to this is a uniform component of scattering; this shows the effect of opacifying a material that is originally without significant scattering. Although frequency (which does not change with n when crossing an interface) is used as the convenient spectral variable in the analysis, the cutoff location is given here in terms of wavelength which is common in the literature. The parameter $\lambda_c T_{g1}$ determines the fractional amounts of energy on either side of λ_c for the blackbody source at T_{g1} on the hot side. The value $\lambda_c T_{g1} = 4000$ is used, which divides the incident radiant energy about equally above and below λ_c. Additional parameters are the individual values of aD and $\sigma_s D$ on either side of λ_c.

Figure 8 shows the effect of adding scattering to a material with $aD = 0.1$ and 10 in the short and long wavelength regions. The two parts of the figure are for $n = 1$ and 2. The dashed curve shows the temperature distribution for absorption only ($\sigma_s D = 0$). Then a constant amount of scattering is added, $\sigma_s D = 0.9$. The temperature distribution, as given by the upper solid curve, is hardly changed by this amount of scattering probably because the layer has small absorption in the short wavelength region. A further increase in scattering to $\sigma_s D = 9.9$ decreases the temperature a moderate amount except for small X where there is a slight increase. This may be caused by backscattering which increases absorption for small X, but otherwise reduces energy penetration to larger X. This effect is increased for $n = 2$. For comparison, two dot-dashed curves are included where absorption has been added, rather than scattering, to provide the same optical thicknesses as for the two solid curves. The relative positions of the solid and dot-dash curves show the effect of part of the optical thicknesses being the result of scattering rather than absorption.

Figures 9a and b give the effect on the temperature profiles of adding scattering of $\sigma_s D = 9$ for all λ to a two-band absorbing layer with $aD = 1$, 100 below and above λ_c. The results are compared to those for absorption only for $n = 1$ and 2. The two-band curve for absorption only ($aD = 1, 100$) is shown with long dashes. This is compared with nonscat-

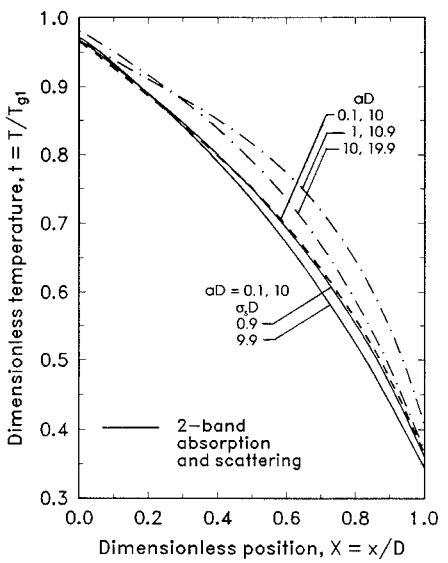

a) $n = 1$

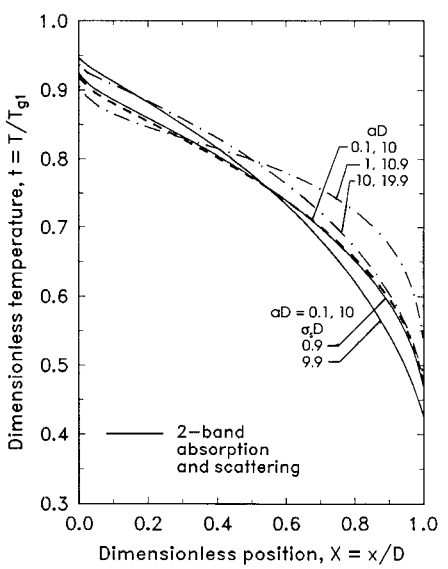

b) $n = 2$

Fig. 8 Nongray and scattering effects on temperature distributions, $t_{s1} = t_{g1} = 1$, $t_{s2} = t_{g2} = 0.25$, $H_R = 1$, $N_D = 0.1$, $R = 1$, $\lambda_c T_{g1} = 4000$, band $aD = 0.1$, 10.

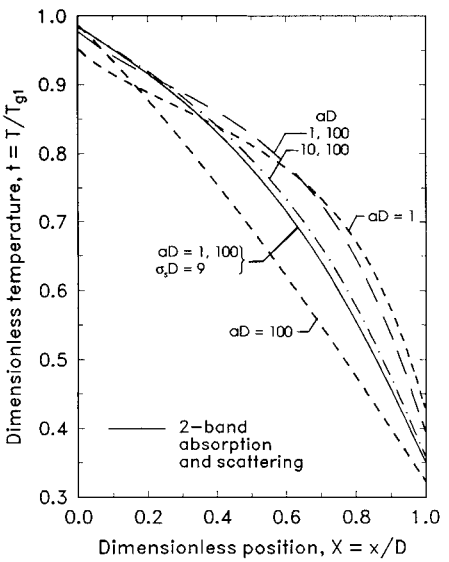

a) $n = 1$

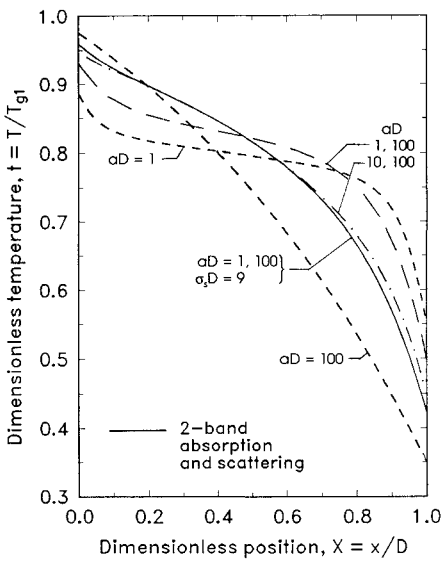

b) $n = 2$

Fig. 9 Nongray and scattering effects on temperature distributions, $t_{s1} = t_{g1} = 1$, $t_{s2} = t_{g2} = 0.25$, $H_R = 1$, $N_D = 0.1$, $R = 1$, $\lambda_c T_{g1} = 4000$, band $aD = 1,100$.

tering gray layers with $aD = 1$ or 100 by the short dashed curves. For $\lambda T_{g1} = 4000$ the two-band curve for $\Omega = 0$ has some of the characteristics that the nonscattering gray curves have for the κ_D in each of the bands. It is shaped like the gray curve for $aD = 1$ ($\Omega = 0$), but is displaced somewhat toward the gray curve for $aD = 100$ ($\Omega = 0$).

When scattering of $\sigma_s D = 9$ is added, the solid curve is obtained. The profile is a little more linear like an opaque layer, such as the gray profile with $aD = 100$ and $\Omega = 0$. A dot-dash curve is shown for absorption only with aD having the same values as $(a + \sigma_s)D$ for the two-band case with scattering; the profile is close to the solid curve. The optical thicknesses are large enough that scattering acts the same as absorption, which is the condition in radiative equilibrium.

Conclusions

Temperature distributions and radiative fluxes are obtained for a semitransparent layer heated on both sides by radiation and convection. Isotropic scattering is included, and both gray and nongray behavior is examined. A refractive index larger than unity significantly affects the temperature distributions by producing internal reflections at the boundaries. Near the boundaries there can be large temperature gradients from the interaction of radiation and convection. For large n the temperatures become somewhat uniform in the central part of the layer.

For a gray layer the effect of scattering was found to depend on the optical thickness and the amount of absorption in the layer. For optically thin layers with $\kappa_D = (a + \sigma_s)D \leq 1$ the temperature profiles depend on the absorption thickness aD and are rather independent of the scattering thickness $\sigma_s D$. For larger $\kappa_D \geq 10$ (and with aD not becoming very small), scattering is almost as effective as additional absorption so the temperature distributions depend on the optical thickness $(a + \sigma_s)D$. A two-band nongray layer exhibits some of this behavior depending on whether both bands are optically thin, optically thick, or one is thin and the other thick.

The energy leaving each surface by emission, scattering, and transmission from the other side was examined to determine when it could be used to calculate the surface temperature as would be done in experimental measurements. For some conditions, an optical thickness of 10 was large enough to obtain an accurate surface temperature. For other parameters, an optical thickness of 30 or larger was required. Increased heat conduction decreases the required optical thickness since internal temperatures become more uniform, and emitted and scattered radiation from within the medium are more characteristic of the surface temperature. For scattering there will be an error in using the leaving energy to predict surface temperature. This is because scattered energy leaving from within the layer may not be characteristic of the surface temperature.

References

[1]Spuckler, C. M., and Siegel, R., "Refractive Index Effects on Radiative Behavior of a Heated Absorbing-Emitting Layer," *Journal of Thermophysics and Heat Transfer*, Vol. 6, No. 4, 1992, pp. 596–604.

[2]Makino, T., Kunitomo, T., Sakai, I., and Kinoshita, H., "Thermal Radiation Properties of Ceramic Materials," *Heat Transfer—Japanese Research*, Vol. 13, Oct.–Dec. 1984, pp. 33–50.

[3]Gardon, R., "Calculation of Temperature Distributions in Glass Plates Undergoing Heat-Treatment," *Journal of the American Ceramic Society*, Vol. 41, No. 6, 1958, pp. 200–209.

[4]Fowle, A. A., Strong, P. F., Comstock, D. F., and Sox, C., "Computer Program to Predict Heat Transfer Through Glass," *AIAA Journal*, Vol. 7, No. 3, 1969, pp. 478–483.

[5]Rokhsaz, F., and Dougherty, R. L., "Radiative Transfer Within a Finite Plane-Parallel Medium Exhibiting Fresnel Reflection at a Boundary," American Society of Mechanical Engineers HTD-Vol. 106, *Heat Transfer Phenomena in Radiation, Combustion and Fires*, 1989, pp. 1–8.

[6]Ping, T. H., and Lallemand, M., "Transient Radiative-Conductive Heat Transfer in Flat Glasses Submitted to Temperature, Flux, and Mixed Boundary Conditions," *International Journal of Heat and Mass Transfer*, Vol. 32, No. 5, 1989, pp. 795–810.

[7]Crosbie, A. L., and Shieh, S. M., "Three-Dimensional Radiative Transfer for Anisotropic Scattering Medium with Refractive Index Greater Than Unity," *Journal of Quantitative Spectroscopy and Radiative Transfer*, Vol. 44, No. 2, 1990, pp. 299–312.

[8]Viskanta, R., and Grosh, R. J., "Heat Transfer by Simultaneous Conduction and Radiation in an Absorbing Medium," *Journal of Heat Transfer*, Vol. 84, No. 1, 1962, pp. 63–72.

[9]Amlin, D. W., and Korpela, S. A., "Influence of Thermal Radiation on the Temperature Distribution in a Semi-Transparent Solid," *Journal of Heat Transfer*, Vol. 101, No. 1, 1979, pp. 76–80.

[10]Tarshis, L. A., O'Hara, S., and Viskanta, R., "Heat Transfer by Simultaneous Conduction and Radiation for Two Absorbing Media in Intimate Contact," *International Journal of Heat and Mass Transfer*, Vol. 12, No. 3, 1969, pp. 333–347.

[11]Anderson, E. E., and Viskanta, R., "Spectral and Boundary Effects on Coupled Conduction-Radiation Heat Transfer Through Semitransparent Solids," *Wärme- and Stoffübertragung*, Vol. 6, No. 1, 1973, pp. 14–24.

[12]Siegel, R., and Howell, J. R., *Thermal Radiation Heat Transfer*, 2nd ed., Hemisphere, Washington, DC, 1981.

[13]Cox, R. L., "Fundamentals of Thermal Radiation in Ceramic Materials," *Thermal Radiation in Solids*, edited by S. Katzoff, NASA SP-55, 1965, pp. 83–101.

[14]Richmond, J. C., "Relation of Emittance to Other Optical Properties," *Journal of Research of the National Bureau of Standards*, Vol. 67C, No. 3, 1963, pp. 217–226.

[15]*Planck's Radiation Functions and Electronic Functions*, Federal Works Agency Works Projects Administration for the City of New York, A. N. Lowan, Technical Director, U.S. National Bureau of Standards Computation Lab., 1941.